

Real-Space Experimental Observation of Magnetic Surface Spirals in FeGe

L. A. Turnbull,^{1,*} M. T. Littlehales,¹ M. N. Wilson,¹ M. T. Birch,² H. Popescu,³ N. Jaouen,³ J. A. T. Verezhak,⁴ G. Balakrishnan,⁴ and P. D. Hatton¹

¹*Department of Physics, Durham University, Durham, DH1 3LE, UK*

²*Max Planck Institute for Intelligent Systems, 70569 Stuttgart, Germany*

³*Synchrotron SOLEIL, Saint Aubin, BP 48, 91192 Gif-sur-Yvette, France*

⁴*Department of Physics, University of Warwick, Coventry, CV4 7AL, UK*

Isotropic helimagnets are known to host a diverse range of chiral magnetic states. In 2016, F.N. Rybakov *et al.* theorized the presence of a surface-pinned stacked spin spiral phase [F.N. Rybakov *et al.*, 2016 New J. Phys. 18 045002], which has yet to be observed experimentally. Here we present experimental evidence for the observation of this state in lamellae of FeGe using resonant x-ray holographic imaging data and micromagnetic simulations. The identification of this state has significant implications for the stability of other coexisting spin textures, and will help complete our understanding of helimagnetic systems.

Broken inversion symmetry in the crystal structure of chiral magnets induces an antisymmetric exchange interaction known as the Dzyaloshinskii-Moriya interaction (DMI) [1, 2]. Competition between the DMI and ferromagnetic exchange interaction in such systems stabilizes a helical ground state, characterized by the incommensurate winding of the magnetization, \mathbf{M} , about a propagation vector (Fig. 1(a)) [3]. These helimagnetic systems have garnered significant interest due to the rich array of spiral structures arising in their magnetization, including chiral soliton lattices in layered CrNb₃S₆ [4] and skyrmion lattices in cubic helimagnets such as MnSi [5, 6], CoZnMn alloys [7, 8] and FeGe [9, 10], the material on which this study focuses. In particular, the topological and transport properties of these emergent magnetic states show the potential for novel applications in advanced spintronic devices [11–14].

The standard model for magnetism in bulk cubic helimagnets takes the form of the energy density functional

$$w = A(\nabla \cdot \mathbf{m})^2 + D\mathbf{m} \cdot (\nabla \times \mathbf{m}) - \mu_0 M_s \mathbf{m} \cdot \mathbf{H}, \quad (1)$$

where the terms represent the exchange interaction with stiffness constant A , DMI with constant D and Zeeman interaction respectively [15, 16]. The external magnetic field vector is \mathbf{H} , while \mathbf{m} is the unit vector in the direction of the local magnetization, $\mathbf{M} = M_s \mathbf{m}$. The bulk magnetic phase diagram arising in these archetypal helimagnetic systems is well established: in an increasing external magnetic field the multi-domain helical ground state transforms into a single-domain conical state propagating parallel to the field direction, before ultimately converging to a saturated ferromagnetic state at a critical field of $H_D = D^2/2AM_s$ [17, 18]. A key result is that the equilibrium period of the conical state and the zero-field helicoid state,

$$L_D = \frac{4\pi A}{|D|}, \quad (2)$$

is determined by the ratio of the exchange stiffness and DMI constant [19]. Magnetocrystalline anisotropy terms

are commonly neglected in this model, due to their comparatively weak contribution.

Finite thickness effects, such as shape anisotropy and exposed sample boundaries, can also significantly modify the local energy landscape. In lamellae of thickness $L \sim L_D$, the magnetization undergoes a field-induced transformation to an equilibrium lattice of skyrmion tubes [20], due to the effect of a chiral surface twisting, which lowers the energy of the skyrmion lattice relative to the conical state [21]. In lamellae thicker than the fundamental period, $L \gtrsim L_D$, stable surface-pinned skyrmions, known as chiral bobbbers, which collapse into Bloch points in the bulk of a sample, have also been observed [22]. Additionally, it has been demonstrated that the helicity of a skyrmion tube is modified from a Bloch character in the bulk of a sample, towards a Néel character at the surface, indicating the diverse range of spiral structures that can emerge in chiral magnets [23, 24].

In 2016, Rybakov *et al.* theorized the existence of surface spiral modulations termed the stacked spin spiral phase (Fig. 1(b)), which coexists with a bulk conical state embedded in isotropic chiral magnets, for $L \geq 4.18L_D$ [25]. The phase is characterized by modulation periods exceeding the fundamental period, L_D , and was predicted to have both Bloch and Néel character, akin to the surface helicity of skyrmions. Here we present resonant x-ray holography data and micromagnetic simulations consistent with the observation of this stacked spin spiral state in lamellae of FeGe.

Resonant x-ray holography is a form of coherent diffractive imaging where the phase information of a magnetic state is encoded in a diffraction pattern by the interference of a reference beam with light scattered in transmission through the sample [26]. This hologram is a reciprocal space map of the sample, and Fourier transforming the hologram reconstructs a real-space holographic image of the magnetization [27]. The magnetic scattering contrast can be resonantly enhanced by tuning the x-ray energy to the L_3 absorption edge of the magnetic atom (Fe- $L_3 = 706$ eV) [28] and components of the mag-

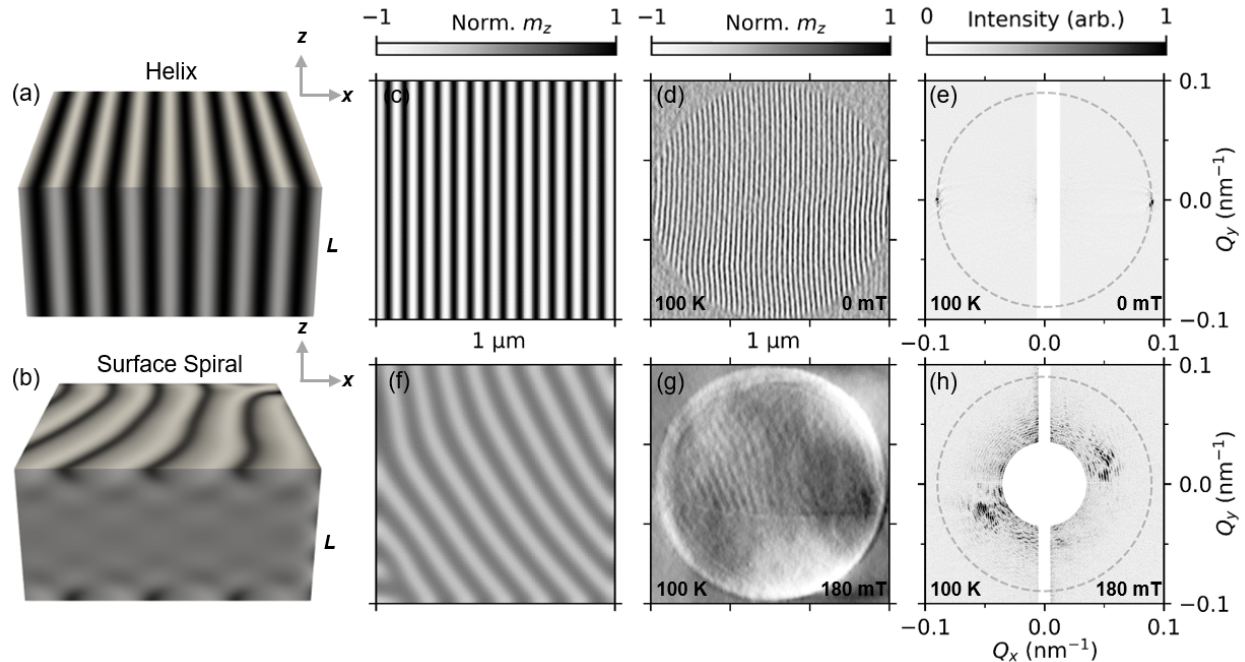


FIG. 1. a) Schematic of a magnetic helical state. b) Schematic of a magnetic surface spiral state. c) Simulated x-ray imaging projection of a magnetic helix. Regions of black (white) represent net magnetization towards (away) from the reader. d) X-ray holographic image of a magnetic helix. e) X-ray scattering hologram of a magnetic helix. The dashed circle marks the q -range for the zero-field helical state. The direct transmission of the beam is masked for clarity. f) Simulated x-ray imaging projection of the surface spiral state. g) X-ray holographic image of a surface spiral state. h) X-ray scattering hologram of a magnetic surface spiral.

netization parallel with the x-ray beam are isolated by utilizing x-ray magnetic circular dichroism (XMCD) [29]. A notable advantage of this technique is that, due to the penetration depths associated with soft x-rays, it is possible to examine samples which are thicker than those available to comparable electron-based magnetic imaging techniques such as Lorentz transmission electron microscopy (LTEM) [30].

Figure 1(a) shows the schematic of a helical state propagating in the x -direction; the corresponding simulated x-ray holographic projection along the z -direction is shown in Fig. 1(c); regions of white and black represent net magnetization towards and away from the reader. Fig. 1(d,e) show the equivalent experimental x-ray scattering holographic image and hologram of such a helical state in a lamella of FeGe. The sample was 200 nm ($L=2.85L_D$) thick and exhibited the expected helical winding period of $L_D = 70 \pm 2$ nm [31]. The purely sinusoidal modulation of this magnetization structure causes an individual helical domain to comprise a single pair of peaks in reciprocal space. As the relevant forms of the exchange and DM interactions are isotropic, this also defines a fixed radius of $2\pi/L_D$, at which all such peaks would be expected to exist, in the absence of higher order anisotropic terms [32]. The dashed circles in Fig. 1(e,h) mark the observed q -value of the zero-field helical state.

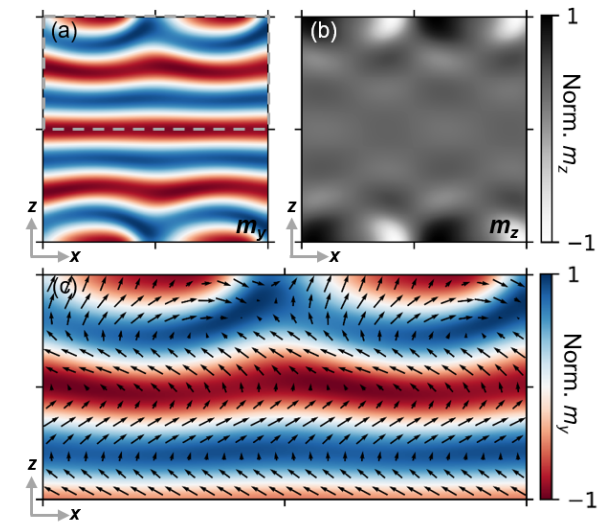


FIG. 2. Stacked Spiral State. a-b) Cross sectional view of the m_y and m_z components of the magnetization for the surface spiral phase. c) Closer schematic view of the surface spiral, corresponding to the region marked in panel 2(a).

Magnetic helices are known to evolve with increasing magnetic field, when pinning due to uniaxial or shape anisotropies resists transition to a conical or field-

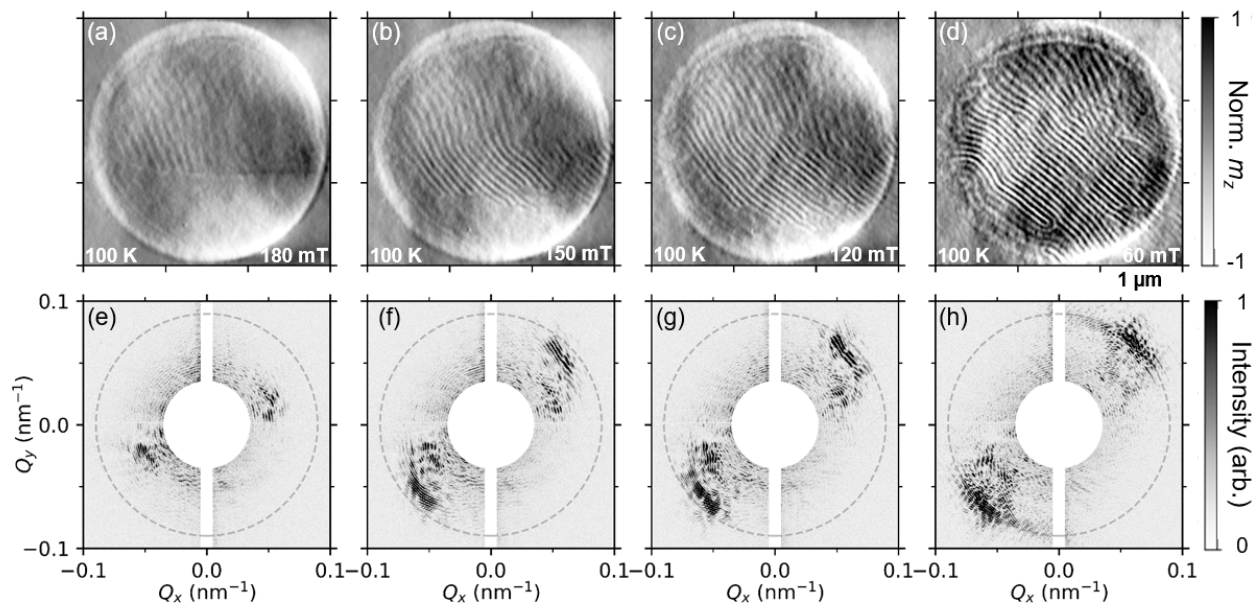


FIG. 3. Field evolution of surface state. a-d) Holographic images of FeGe lamellae with the applied magnetic field marked on each sub-figure. e-f) Corresponding XMCD scattering holograms. The dashed circles marks the q -range for the zero-field helical state. The direct transmission of the beam is masked for clarity.

polarized state [33, 34], forming a distorted helicoid with an increased period. In out-of-plane magnetic fields we observe a longer period modulated state, however it does not match the expected distortion of helices in an applied field, and instead shows significant similarities to the surface spiral state predicted by Rybakov *et al.* [25]. A holographic image and scattering pattern of such a modulated state with an extended period in a 300 nm thick ($L=4.3L_D$) lamella of FeGe are shown in Fig. 1(g,h). The state was produced by zero field cooling from above the Curie temperature ($T_C = 278 \pm 1$ K), to 100 K, increasing the out-of-plane magnetic field to saturation and then decreasing the field at fixed temperature to 180 mT. The bottom half of the image has no modulated contrast, consistent with an out-of-plane conical or field-polarized state. However, the top region of the image shows a series of low contrast, long-period modulations. The peaks in the scattering hologram correspond to an ordering period of $1.8L_D$.

Figure 1(f) shows the x-ray projection of a simulated surface spiral state stabilized in a $1 \times 1 \mu\text{m}^2$ region, which emerged when relaxing a pure out-of-plane conical state in our micromagnetic simulations [35] using FeGe material parameters [36]. This projection shows strong qualitative similarities with the holographic image of Fig. 1(g) and exhibits the same ordering behaviour as the scattering hologram.

Figure 2 shows cross-sectional views of the m_y and m_z components of this simulated surface state. The horizontal stripes in the middle of Fig. 2(a) are representative of an out-of-plane conical state, while the top and bottom

surfaces show extended period modulations, which decay into the bulk of the sample. In a semi-infinite crystal one would expect the magnetization to transition into a pure conical state, however in lamellae of this thickness range the surface-induced modulation penetrates through the majority of the sample, which can be seen in the weak checker-board pattern occurring throughout Fig 2(b). For a pure conical state propagating in the z -direction with a fixed cone angle, one would not expect any modulated contrast in the m_z component.

Another notable feature of this surface state is that it does not exhibit a purely helical winding, but rather has a mixed cycloidal and helical winding (as shown in the closer schematic view of Fig. 2(c)) – akin to the helicity of skyrmion tubes changing towards a Néel character at the surface [23]. The complex spiral structure of this state necessitates higher-order Fourier components than those visible in Fig. 1(h), however their amplitudes are significantly lower than the visible first-order peaks, and one would therefore not expect to readily observe them within our experimental noise floor. Although it is not possible to fully resolve the helicity of this state from our experimental imaging alone, future work with tomographic x-ray measurements or complementary measurements from techniques such as LTEM or magnetic force microscopy would be able to do so.

To further investigate this state, Figure 3 shows holographic images and the corresponding scattering holograms of the sample in a continuing downward field sweep from the 180 mT state of Fig 1(g). When reducing the field the original region of long periodicity remains, how-

ever, a shorter-wavelength state also emerges in the bottom section of the image. As the field sweep continues downward, the shorter-wavelength state occupies an increasingly large volume fraction of the sample and its period relaxes towards the fundamental helimagnetic period, while the surface spiral region remains at a higher period. This is consistent with the behaviour of a common helicoidal state, which is more energetically stable than an out-of-plane conical state in lower magnetic fields. The helicoidal state is also lower in energy than the surface spiral at zero field, except in the limit $L/L_D \rightarrow \infty$ [25].

The other notable feature of this helicoidal state is that it increases in contrast relative to the long-period state. As all of the images are equivalently normalized, this is indicative of a higher volume fraction of the magnetization aligning parallel with the beam, consistent with the helicoid occupying the full volume of the sample, while the long-period spiral state only generates significant contrast at the surfaces. Surface induced modulations are expected to exhibit an exponential decay into the bulk of a sample over length scales comparable to L_D [37]. The two states also appear to continuously merge into each other, with bifurcation defects mediating the changing wavelength. This could indicate a continuity of striped modulations on the surface, but a difference in how far the underlying states penetrate into the bulk of the sample. It gives the appearance that the helicoids nucleate from the surface state, before growing into the bulk.

Figure 4(a) shows the field dependence of the periodicity of both states. The solid red (purple) lines show the well documented theoretical periods for the helicoid (conical) state [33, 34], while the blue line shows the theoretical surface spiral period from Rybakov *et al.* [25]. This data shows that the field dependence of the two states is significantly different, and that the longer wavelength state matches the predictions of Rybakov *et al.* for the surface spiral. This gives significant additional evidence that this long-wavelength state is the predicted surface spiral state.

Figure 4(b) shows the average peak to peak contrast of both states as a function of field. The surface spiral shows a linear trend, which could indicate either an increasing volume fraction with decreasing field, or an evolution of the fundamental structure of the surface spiral, increasing the surface magnetization parallel with the probe beam. Notably, the helicoid initially exhibits the same contrast as the surface state at 160 and 120 mT, within error, before ultimately saturating at the higher zero-field signal, while at 60 mT the surface spiral contrast remains low. This is further evidence that the helicoid state could nucleate out from the surface spiral, before penetrating further into the depths of the sample.

To conclude, x-ray holography was used in this study to observe a low-contrast modulated magnetic state with a period exceeding the fundamental helical period of

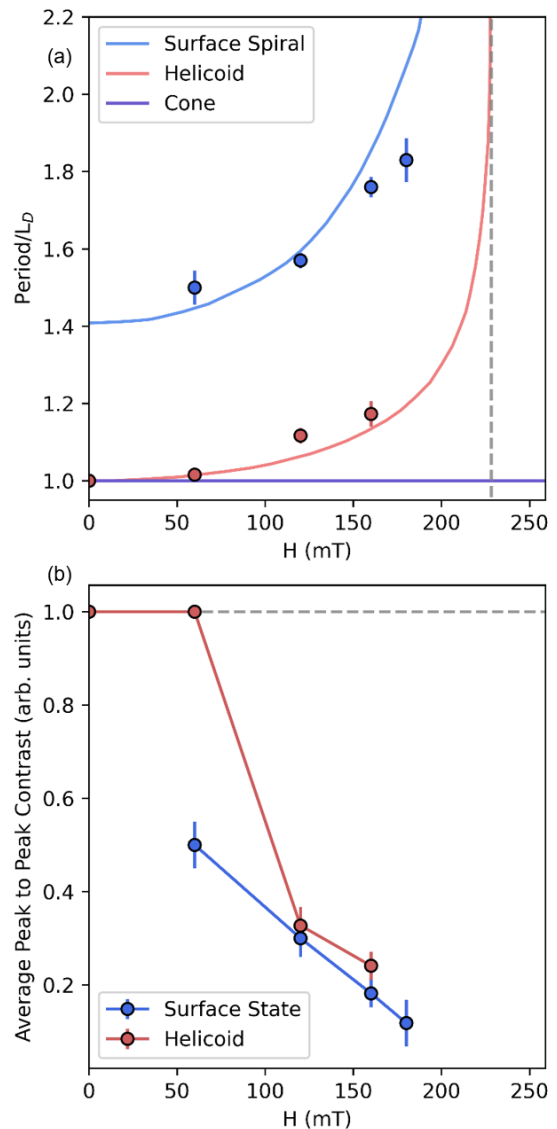


FIG. 4. Period and contrast of the surface state. a) Periodicity of the surface spiral (blue), helicoids (red) and conical (purple) state as a function of applied field. The solid lines correspond to the well established solutions for the period of helicoids and cones [33, 34] and the blue line comes from the periodicity established by Rybakov *et al.* b) The equivalently normalized average peak-to-peak contrast of the respective states.

FeGe, that coexists with magnetic helices. This state is consistent with predictions of the stacked spiral surface state by Rybakov *et al.* in 2016, demonstrating that this state does exist. This observation is significant as it likely means that a similar surface state is present in each of the wide array of isotropic chiral magnetic systems currently under investigation. The presence of such a surface state will modify the behaviour of other spin textures in these materials (such as skyrmions), and fully investigating it will be necessary for an accurate understanding of these

materials. Depth-dependent studies, such as scattering in reflection geometry or tomographic imaging could be used to map the 3D structure of this state in such future work.

This work was supported by the UK Skyrmion Project EPSRC Programme Grant (EP/N032128/1). We acknowledge SOLEIL for provision of synchrotron radiation facilities and we would like to thank H. Popescu and N. Jaouen for assistance in using beamline SEXTANTS. We acknowledge Diamond Light Source for time on Beamline I10 under Proposal MM27196-1. We acknowledge the GJ Russell Microscopy Facility for provision of focused ion-beam microscopes.

* l.a.turnbull@durham.ac.uk

- [1] I. Dzyaloshinsky, *Journal of Physics and Chemistry of Solids* **4**, 241 (1958).
- [2] T. Moriya, *Phys. Rev.* **120**, 91 (1960).
- [3] J. Beille, J. Voiron, and M. Roth, *Solid State Communications* **47**, 399 (1983).
- [4] Y. Togawa, T. Koyama, K. Takayanagi, S. Mori, Y. Kousaka, J. Akimitsu, S. Nishihara, K. Inoue, A. S. Ovchinnikov, and J. Kishine, *Phys. Rev. Lett.* **108**, 107202 (2012).
- [5] S. Mühlbauer, B. Binz, F. Jonietz, C. Pfleiderer, A. Rosch, A. Neubauer, R. Georgii, and P. Böni, *Science* **323**, 915 (2009).
- [6] X. Yu, A. Kikkawa, D. Morikawa, K. Shibata, Y. Tokunaga, Y. Taguchi, and Y. Tokura, *Phys. Rev. B* **91**, 054411 (2015).
- [7] Y. Tokunaga, X. Z. Yu, J. S. White, H. M. Rønnow, D. Morikawa, Y. Taguchi, and Y. Tokura, *Nature Communications* **6**, 7638 (2015).
- [8] K. Karube, J. S. White, V. Ukleev, C. D. Dewhurst, R. Cubitt, A. Kikkawa, Y. Tokunaga, H. M. Rønnow, Y. Tokura, and Y. Taguchi, *Phys. Rev. B* **102**, 064408 (2020).
- [9] X. Yu, N. Kanazawa, Y. Onose, K. Kimoto, W. Zhang, S. Ishiwata, Y. Matsui, and Y. Tokura, *Nature Mater.* **10**, 106 (2011).
- [10] J. Tang, Y. Wu, W. Wang, L. Kong, B. Lv, W. Wei, J. Zang, M. Tian, and H. Du, *Nature Nanotechnology* (2021), 10.1038/s41565-021-00954-9.
- [11] R. Tomasello, E. Martinez, R. Zivieri, L. Torres, M. Carpentieri, and G. Finocchio, *Sci. Rep.* **4**, 6784 (2014).
- [12] J. Zázvorka, F. Jakobs, D. Heinze, N. Keil, S. Kromin, S. Jaiswal, K. Litzius, G. Jakob, P. Virnau, D. Pinna, K. Everschor-Sitte, L. Rózsa, A. Donges, U. Nowak, and M. Kläui, *Nature Nanotech* **14**, 658 (2019).
- [13] K. M. Song, J.-S. Jeong, B. Pan, X. Zhang, J. Xia, S. Cha, T.-E. Park, K. Kim, S. Finizio, J. Raabe, J. Chang, Y. Zhou, W. Zhao, W. Kang, H. Ju, and S. Woo, *Nature Electronics* **3**, 148 (2020).
- [14] C. Back, V. Cros, H. Ebert, K. Everschor-Sitte, A. Fert, M. Garst, T. Ma, S. Mankovsky, T. L. Monchesky, M. Mostovoy, N. Nagaosa, S. S. P. Parkin, C. Pfleiderer, N. Reyren, A. Rosch, Y. Taguchi, Y. Tokura, K. von Bergmann, and J. Zang, *Journal of Physics D: Applied Physics* **53**, 363001 (2020).
- [15] P. Bak and M. H. Jensen, *Journal of Physics C: Solid State Physics* **13**, L881 (1980).
- [16] N. Nagaosa and Y. Tokura, *Nature Nanotechnology* **8**, 899 (2013).
- [17] B. Lebech, J. Bernhard, and T. Freltoft, *Journal of Physics: Condensed Matter* **1**, 6105 (1989).
- [18] S. Buhrandt and L. Fritz, *Phys. Rev. B* **88**, 195137 (2013).
- [19] A. Bogdanov and A. Hubert, *Journal of Magnetism and Magnetic Materials* **138**, 255 (1994).
- [20] M. T. Birch, D. Cortés-Ortuño, L. A. Turnbull, M. N. Wilson, F. Groß, N. Träger, A. Laurenson, N. Bukin, S. H. Moody, M. Weigand, G. Schütz, H. Popescu, R. Fan, P. Steadman, J. A. T. Verezhak, G. Balakrishnan, J. C. Loudon, A. C. Twitchett-Harrison, O. Hovorka, H. Fangohr, F. Y. Ogrin, J. Gräfe, and P. D. Hatton, *Nature Communications* **11**, 1726 (2020).
- [21] F. N. Rybakov, A. B. Borisov, and A. N. Bogdanov, *Phys. Rev. B* **87**, 094424 (2013).
- [22] F. Zheng, F. N. Rybakov, A. B. Borisov, D. Song, S. Wang, Z.-A. Li, H. Du, N. S. Kiselev, J. Caron, A. Kovács, M. Tian, Y. Zhang, S. Blügel, and R. E. Dunin-Borkowski, *Nature Nanotechnology* **13**, 451 (2018).
- [23] S. L. Zhang, G. van der Laan, W. W. Wang, A. A. Haghighirad, and T. Hesjedal, *Phys. Rev. Lett.* **120**, 227202 (2018).
- [24] F. Zheng, F. N. Rybakov, N. S. Kiselev, D. Song, A. Kovács, H. Du, S. Blügel, and R. E. Dunin-Borkowski, *Nature Communications* **12**, 5316 (2021).
- [25] F. N. Rybakov, A. B. Borisov, S. Blügel, and N. S. Kiselev, *New Journal of Physics* **18**, 045002 (2016).
- [26] S. Eisebitt, J. Lüning, W. Schlotter, M. Lörger, O. Hellwig, W. Eberhardt, and J. Stöhr, *Nature* **432**, 885 (2004).
- [27] D. Zhu, M. Guizar-Sicairos, B. Wu, A. Scherz, Y. Acremann, T. Tylliszczak, P. Fischer, N. Friedenberger, K. Ollefs, M. Farle, J. R. Fienup, and J. Stöhr, *Phys. Rev. Lett.* **105**, 043901 (2010).
- [28] M. Blume and D. Gibbs, *Phys. Rev. B* **37**, 1779 (1988).
- [29] G. Van der Laan and A. I. Figueroa, *Coordination Chemistry Reviews* **277**, 95 (2014).
- [30] C. Phatak, A. Petford-Long, and M. De Graef, *Current Opinion in Solid State and Materials Science* **20**, 107 (2016).
- [31] D. M. Burn, S. L. Zhang, S. Wang, H. F. Du, G. van der Laan, and T. Hesjedal, *Phys. Rev. B* **100**, 184403 (2019).
- [32] V. Ukleev, O. Utesov, L. Yu, C. Luo, K. Chen, F. Radu, Y. Yamasaki, N. Kanazawa, Y. Tokura, T.-h. Arima, and J. S. White, *Phys. Rev. Research* **3**, 013094 (2021).
- [33] Y. A. Izyumov, *Soviet Physics Uspekhi* **27**, 845 (1984).
- [34] M. N. Wilson, M. T. Birch, A. Štefančič, A. C. Twitchett-Harrison, G. Balakrishnan, T. J. Hicken, R. Fan, P. Steadman, and P. D. Hatton, *Phys. Rev. Research* **2**, 013096 (2020).
- [35] M. Beg, M. Lang, and H. Fangohr, *IEEE Transactions on Magnetics*, 1 (2021).
- [36] M. Beg, R. A. Pepper, D. Cortés-Ortuño, B. Atie, M.-A. Bisotti, G. Downing, T. Kluyver, O. Hovorka, and H. Fangohr, *Scientific Reports* **9**, 7959 (2019).
- [37] S. A. Meynell, M. N. Wilson, H. Fritzsche, A. N. Bogdanov, and T. L. Monchesky, *Phys. Rev. B* **90**, 014406 (2014).